nature catalysis

SUPPLEMENTARY INFORMATION

https://doi.org/10.1038/s41929-019-0402-8

In the format provided by the authors and unedited.

Confined local oxygen gas promotes electrochemical water oxidation to hydrogen peroxide

Chuan Xia[1,2,9], Seoin Back[3,9], Stefan Ringe[3,9], Kun Jiang[4], Fanhong Chen[5], Xiaoming Sun[5], Samira Siahrostami[6*], Karen Chan[7*] and Haotian Wang[1,8*]

[1]Department of Chemical and Biomolecular Engineering, Rice University, Houston, TX, USA. [2]Smalley-Curl Institute, Rice University, Houston, TX, USA. [3]SUNCAT Center for Interface Science and Catalysis, Department of Chemical Engineering, Stanford University, Stanford, CA, USA. [4]School of Mechanical Engineering, Shanghai Jiaotong University, Shanghai, China. [5]State Key Laboratory of Chemical Resource Engineering, College of Energy, and Beijing Advanced Innovation Centre for Soft Matter Science and Engineering, Beijing University of Chemical Technology, Beijing, China. [6]Department of Chemistry, University of Calgary, Calgary, Alberta, Canada. [7]Department of Physics, Technical University of Denmark, Kongens, Lyngby, Denmark. [8]Canadian Institute for Advanced Research, Toronto, Ontario, Canada. [9]These authors contributed equally: Chuan Xia, Seoin Back, Stefan Ringe. *e-mail: samira.siahrostami@ucalgary.ca; kchan@fysik.dtu.dk; htwang@rice.edu

Confined local oxygen gas promotes electrochemical water oxidation to hydrogen peroxide

Chuan Xia[a,b]† Seoin Back[c]†, Stefan Ringe[c]†, Kun Jiang[d], Fanhong Chen[e], Xiaoming Sun[e], Samira Siahrostami[f,]*, Karen Chan[g,]*, and Haotian Wang[a,]*

[a]*Department of Chemical and Biomolecular Engineering, Rice University, Houston, TX 77005, United States*

[b]*Smalley-Curl Institute, Rice University, Houston, TX 77005, United States*

[c]*SUNCAT Center for Interface Science and Catalysis, Department of Chemical Engineering, Stanford University, Stanford, CA 94305, USA*

[d]*School of Mechanical Engineering, Shanghai Jiaotong University, Shanghai 200240, China*

[e]*State Key Laboratory of Chemical Resource Engineering, College of Energy, and Beijing Advanced Innovation Centre for Soft Matter Science and Engineering, Beijing University of Chemical Technology, 100029 Beijing, China*

[f]*Department of Chemistry, University of Calgary, 2500 University Drive NW, Calgary, Alberta, Canada T2N 1N4*

[g]*Department of Physics, Technical University of Denmark, Kongens Lyngby, Denmark 2800*

[h]*Azrieli Global Scholar, Canadian Institute for Advanced Research (CIFAR), Toronto, Ontario M5G 1M1, Canada*

†contributed equally
*corresponding authors:
samira.siahrostami@ucalgary.ca; kchan@fysik.dtu.dk; htwang@rice.edu

This file includes

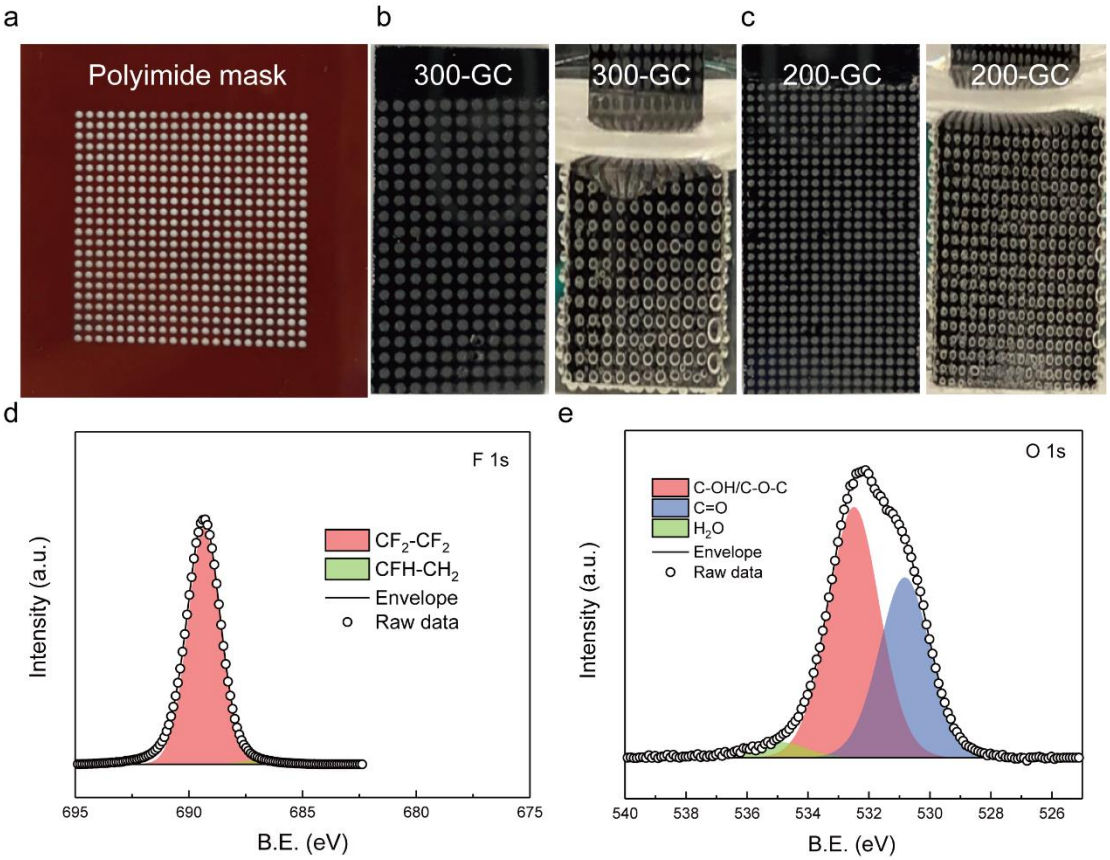

Supplementary Figure 1 | Characterization of PTFE patterned glassy carbon electrodes. a) digital image for laser engraved polyimide shadow mask. **b)** digital photos for 300-GC recorded at open circuit and 2.05 V *vs.* RHE. **c)**, digital photos for 200-GC recorded at open circuit and 2.05 V *vs.* RHE. **d)**, high-resolution F 1*s* XPS spectra for 200-GC catalyst. Two peaks originating from C_xF_y species are detected, the dominated one at 689.3 eV is due to fully fluorinated PTFE $(\text{-}CF_2\text{-}CF_2\text{-})_n$[1]. The minor peak located at 686.9 eV can be ascribed to partially fluorinated carbon chains $(\text{-}CFH\text{-}CH_2\text{-})_n$[1]. **e)**, high-resolution XPS spectra of O 1*s* for 200-GC catalyst. The O 1*s* region was deconvoluted into three contributions at 530.8, 532.5 and 535.1 eV, corresponding to the C=O, C-OH/C-O-C and chemisorbed H_2O, respectively[2-4].

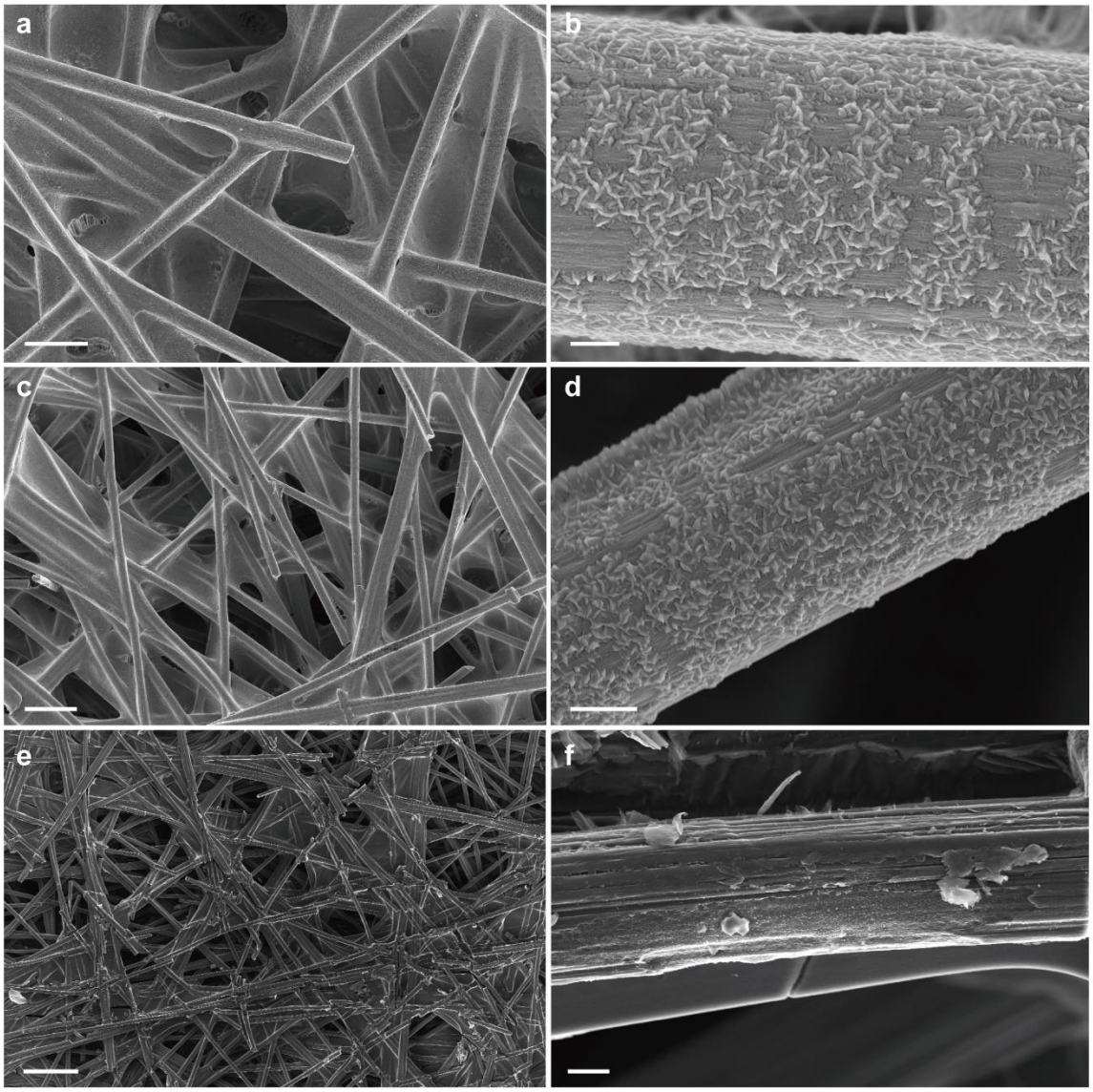

Supplementary Figure 2 | SEM characterization of 60% PTFE modified CFP. a-b, as-prepared CFP-60% catalyst. Obviously, the PTFE nanoflakes have been deposited onto carbon catalyst surface which can provide a very high local O_2 concentration during water oxidation process. Further, undoubtedly, sufficient triple phase contact points can be achieved after PTFE nanoflakes modifications, ensuring the high production rate of H_2O_2. **c-d**, CFP-60% after electrochemical measurements. It shows that the CFP-60% catalysts can maintain their original morphology even after 7-hour stability measurements, implying their good stability towards two-electron water oxidation. **e-f**, CFP-60% catalyst after Argon annealing at 900 °C for 1 hour, leading to the formation of fluorine-doped carbon/CFP electrode. Scale bars: **a** 20 μm; **b** 1 μm; **c** 20 μm; **d** 4 μm; **e** 100 μm; **f** 2 μm.

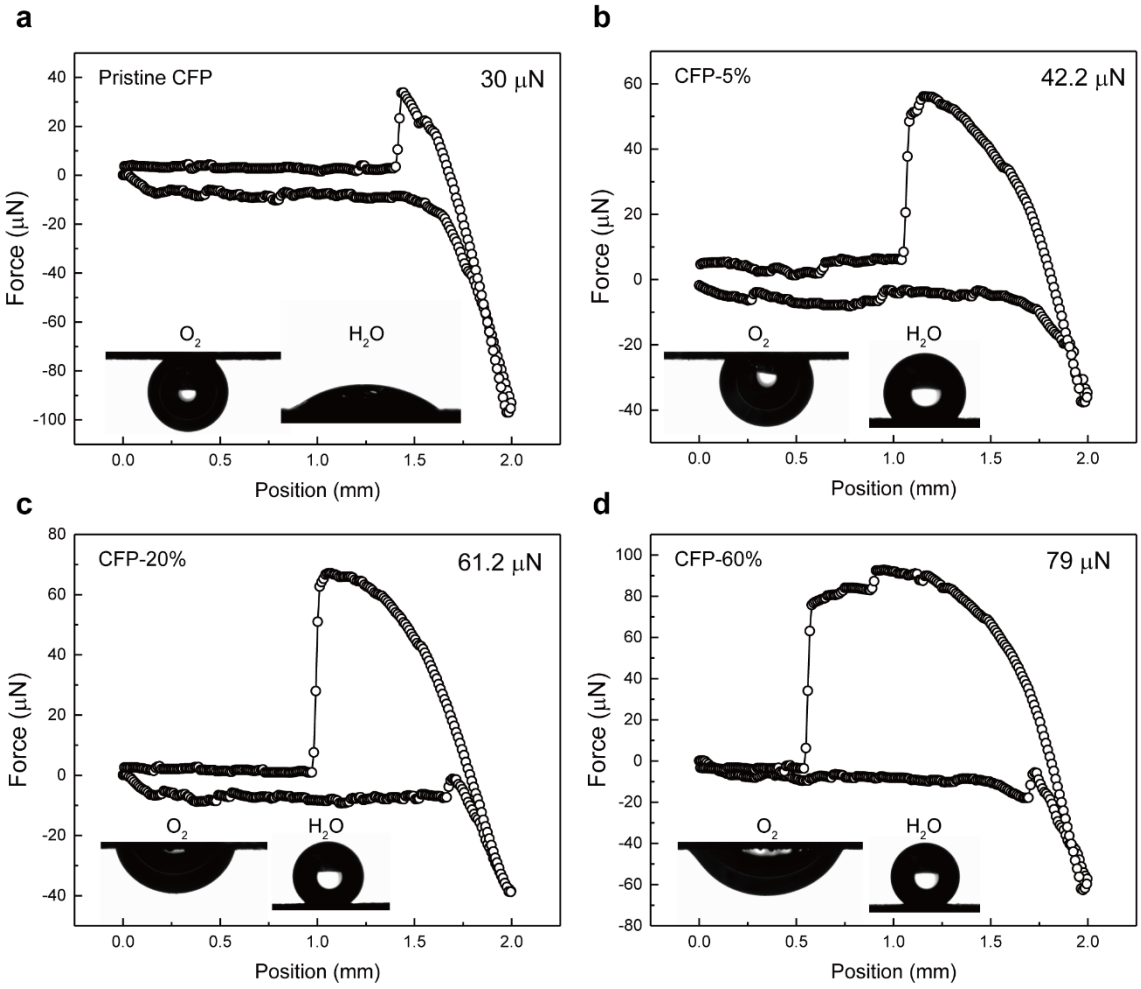

Supplementary Figure 3 | Under-electrolyte O_2 bubble adhesive force measurements for pristine and PTFE modified CFP and the corresponding under-electrolyte O_2 contact angle and in-air water contact angle. a, pristine CFP. **b**, CFP-5%. **c**, CFP-20%. **d**, CFP-60%. The bubble contact angles under electrolyte for pristine CFP, CFP-5%, CFP-20% and CFP-60% were measured as 140.0° ± 2.0°, 116.2° ± 1.1°, 73.5° ± 2.3°, 60.1° ± 1.5°, respectively. The in-air water contact angles for pristine CFP, CFP-5%, CFP-20% and CFP-60% were measured as 37.1° ± 1.8°, 124.2° ± 1.2°, 136.7° ± 0.8°, 142.0° ± 0.5°, respectively.

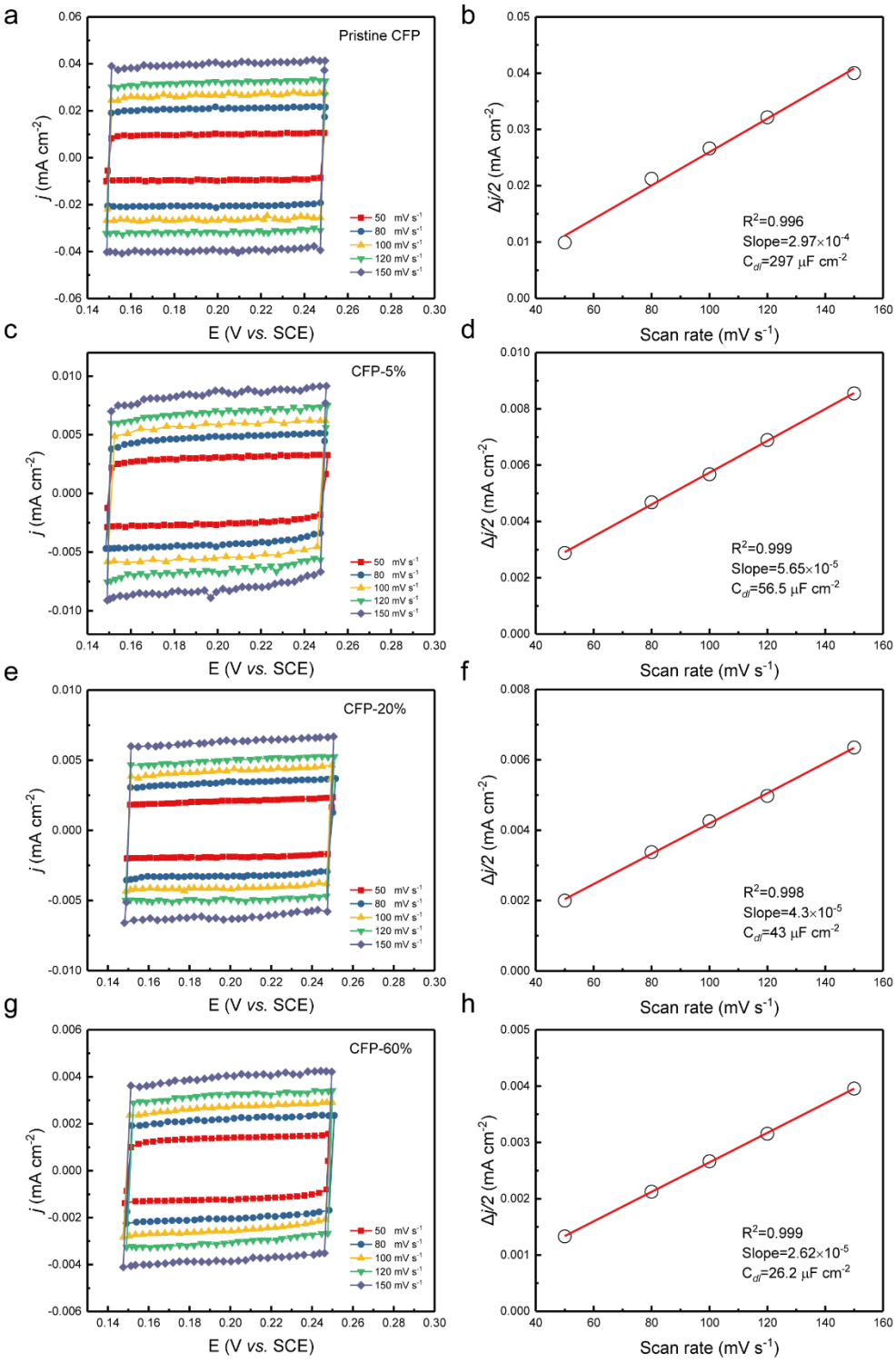

Supplementary Figure 4 | Double-layer capacitance measurements for pristine and PTFE modified CFP. a-b, pristine CFP. **c-d**, CFP-5%. **e-f**, CFP-20%. **g-h**, CFP-60%.

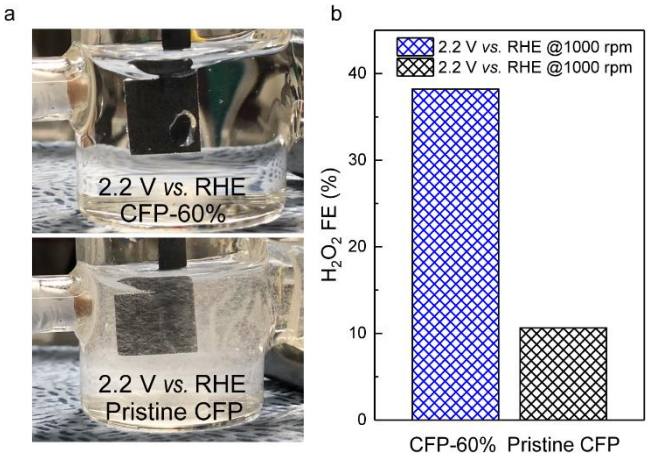

Supplementary Figure 5 | Microscopic stirring effect for pristine and PTFE modified CFP. a, Digital photo of pristine CFP and CFP-60% catalyst during water oxidation at 2.2 V *vs.* RHE, **b**, and the corresponding H_2O_2 FE. Hydrogen peroxide (*OOH species on the electrode) is very hydrophilic and it easily move over the water phase facing with the electrode, competing with the successive further two-electron oxidation on the electrode. When the water phase is covering over the electrode surface the moving motion of H_2O_2 is substantial and could be competing with the subsequent two-electron oxidation. Thus, the vigorous evolution of O_2 bubbles in the region (E > 2.15 V) would cause a sort of microscopic stirring effect to refresh the water coverage, which may be thought to promote the two-electron water oxidation. To exclude this possibility, we performed control experiments. First of all, our results show that the modification of the electrode surface by PTFE would cause a repulsive effect against the aqueous electrolyte (Supplementary Fig. 3), leading to less liquid water covering over the electrode surface for CFP-60% catalyst compared to pristine CFP. If the above proposed mechanism is correct, it is easier for hydrophilic H_2O_2 to escape into water on the surface of pristine CFP and results in a higher H_2O_2 selectivity. This is however the reverse trend compared to our experimental results. Secondly, after modification of PTFE, the CFP-60% catalyst traps generated O_2 gas on the surface, preventing a violent O_2 bubble evolution and release as observed in pristine CFP. This as a result weakens the sort of microscopic stirring effect to refresh the water coverage near the active sites as mentioned by the reviewer (Supplementary Fig. 5a). However, the CFP-60% catalyst presented significantly improved H_2O_2 selectivity compared to pristine CFP (Supplementary Fig. 5b). The above two points excludes the possible explanation that, the vigorous evolution of O_2 bubbles to refresh the water coverage could promote the two-electron water oxidation.

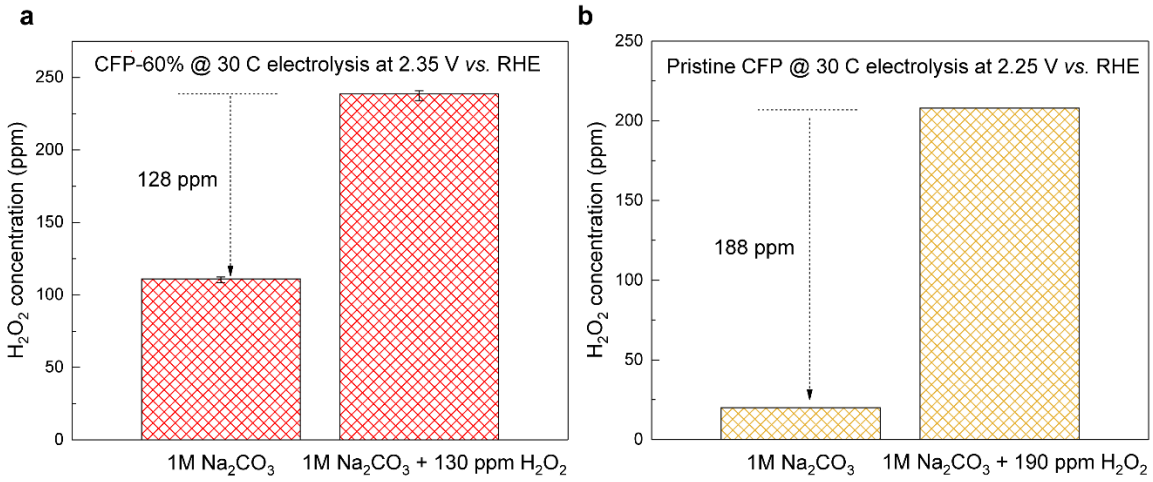

Supplementary Figure 6 | Two-electron water oxidation performance for pristine and PTFE modified CFP in different electrolyte. a, H_2O_2 concentration for CFP-60% catalyst after 30 C charge electrolysis under 2.35 V vs. RHE using different electrolyte. The error bars represent three independent samples. **b**, H_2O_2 concentration for CFP-60% catalyst after 30 C charge electrolysis under 2.35 V vs. RHE using different electrolyte. The error bars represent three independent samples. The free H_2O_2 in the electrolyte might be further oxidized into O_2 during water oxidation, and the hydrophilic CFP and hydrophobic PTFE-CFP could perform differently. Here we included additional experiments and analysis to study this possibility. As all of our experiments were performed under violent stirring, the generated H_2O_2 would diffuse into bulk electrolyte rapidly without local accumulations. The typical concentration of generated H_2O_2 in the electrolyte during our catalyst test is less than 300 ppm. Under this low concentration, the possible oxidation of H_2O_2 would be negligible. Here we designed additional experiments to validate that the generated free H_2O_2 in the electrolyte will not be oxidized into O_2 during water oxidation (Supplementary Fig. 6). First, we used the hydrophobic CFP-60% catalyst to perform water oxidation reaction (passing 30 C charge) in 1.0 M Na_2CO_3 and 1.0 M Na_2CO_3 with 130 ppm H_2O_2 electrolyte under the same operation conditions. As shown in Supplementary Fig. 6a, the H_2O_2 concentration after catalysis is 111 and 239 ppm in these two electrolyte, respectively, with a difference of 128 ppm, matching well with the added 130 ppm concentration. This result clearly demonstrates that the free H_2O_2 in the electrolyte would not be oxidized into O_2 during water oxidation on CFP-60% catalyst. Our second experiment in Supplementary Fig. 6b is like the first one but with the catalyst of the hydrophilic pristine CFP. The result is the same, that the generated free H_2O_2 would not be oxidized by CFP electrode and thus does not contribute to the difference in H_2O_2 selectivity.

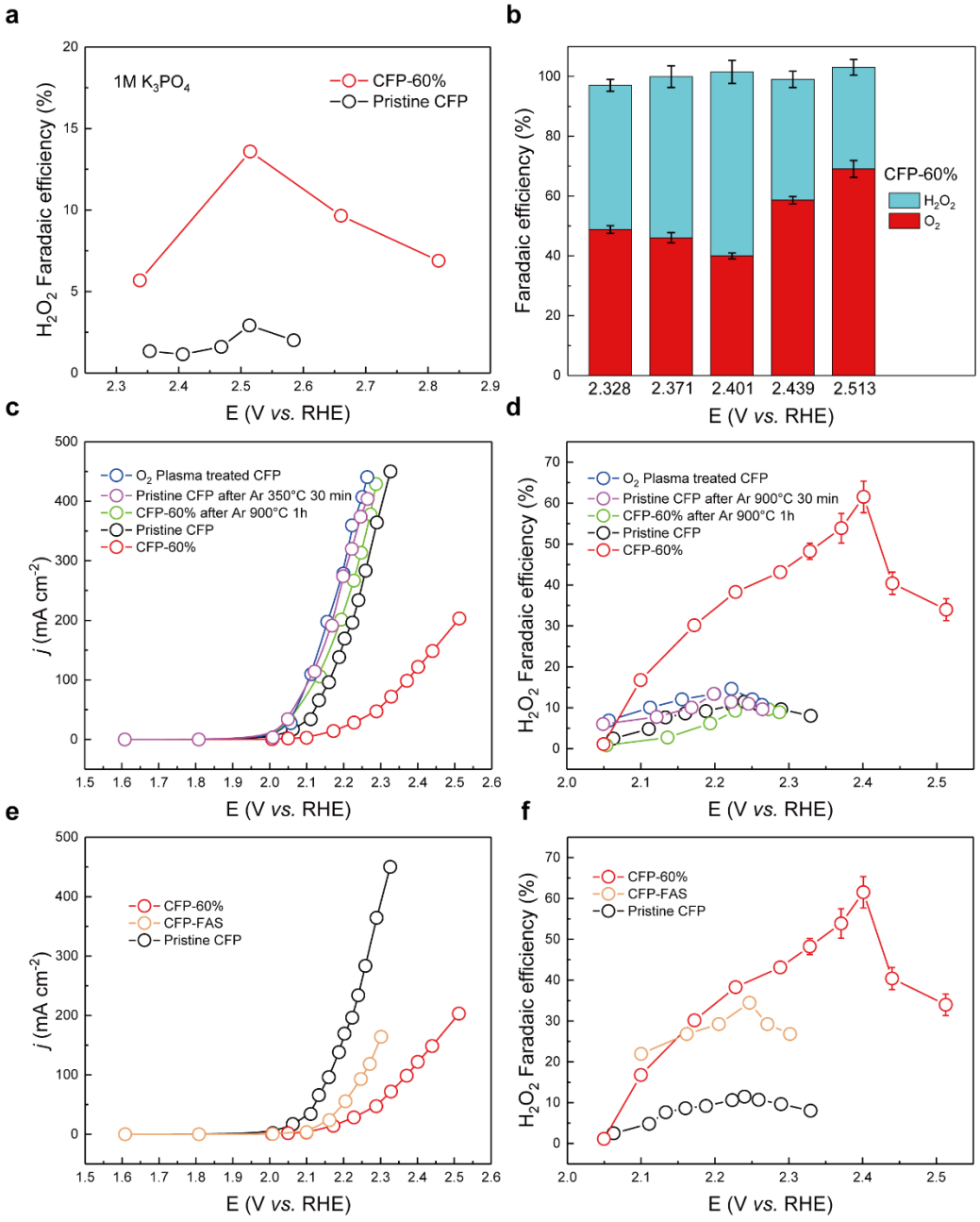

Supplementary Figure 7 | Electrocatalytic H_2O-to-H_2O_2 performance of CFP-60% and the collective control experiments to confirm the local product concentration effect. a, two-electron water oxidation performance of CFP-60% and pristine CFP in 1.0 M K_3PO_4. The results reveal approximate 500% increasement in H_2O_2 Faradaic efficiency from pristine CFP to CFP-60%. **b**, Faradaic efficiencies of H_2O_2 and O_2 on CFP-60% under different potentials. **c-d**, the overall current densities and corresponding H_2O_2 Faradaic efficiencies of pristine, O_2 plasma treated, Argon annealed, fluorine-doped and PTFE decorated CFP electrodes. **e-f**, the overall current density and corresponding H_2O_2 Faradaic efficiency for (1H,1H,2H,2H-heptadecafluorodecyl) silane modified CPF electrode. The data for CFP-60% and pristine CFP are included for comparison.

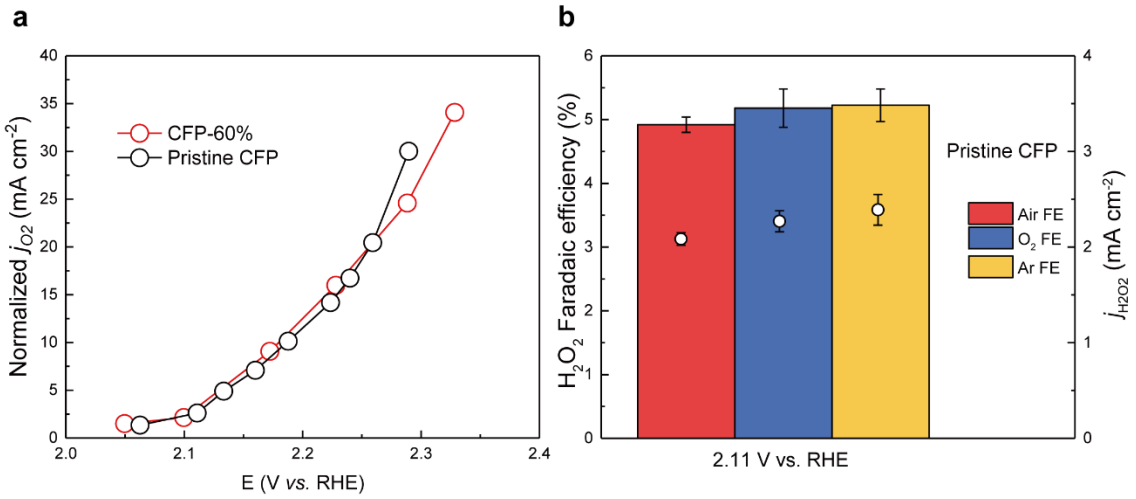

Supplementary Figure 8 | Electrochemical measurements of CFP based electrodes. a, ECSA-normalized partial current of O_2 under different applied potential. **b**, two-electron water oxidation performance of pristine CFP in different gas saturated 1.0 M electrolyte, which shows very similar performance.

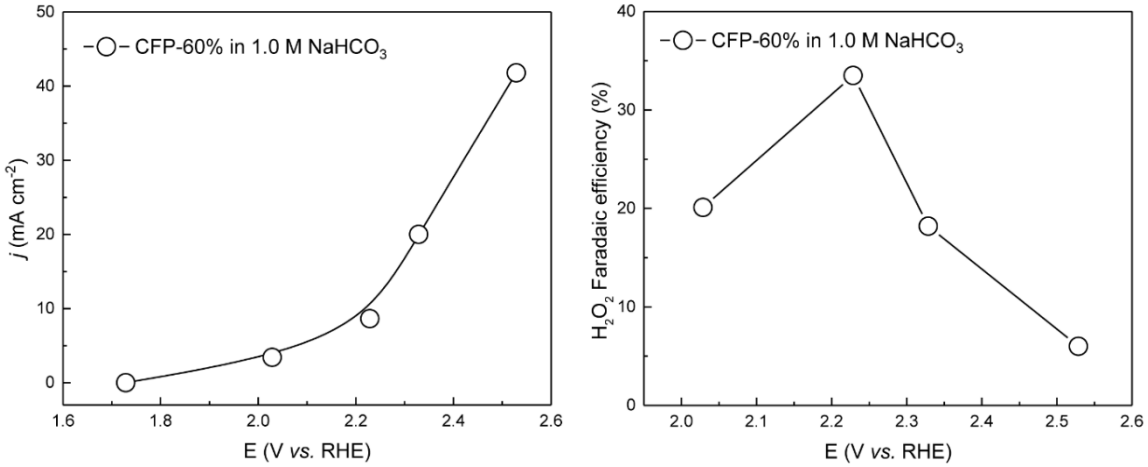

Supplementary Figure 9 | The two-electron water oxidation performance of CFP-60% in 1.0 M $NaHCO_3$ electrolyte and the corresponding H_2O_2 FE. We use the Na_2CO_3 solution as the major electrolyte in our study since we achieved better H_2O-to-H_2O_2 performance by using Na_2CO_3 compared to other electrolytes, such as $NaHCO_3$. We have evaluated our CFP-60% catalyst in 1.0 M $NaHCO_3$, (Supplementary Fig. 9). Different from the observations in previous reports, our carbon catalyst shows lower H_2O-to-H_2O_2 performance in $NaHCO_3$ electrolyte compared to Na_2CO_3. To be specific, CFP-60% delivers a maximal H_2O_2 FE of ~ 66% at 2.4 V *vs.* RHE in Na_2CO_3 electrolyte with a H_2O_2 partial current of 75.2 mA cm^{-2}. However, the maximal H_2O_2 FE for CFP-60% is only ~ 33% in $NaHCO_3$ electrolyte at 2.25 V *vs.* RHE with lower H_2O_2 partial current of 2.9 mA cm^{-2}. In our case, we do not observe the promotion effect on H_2O_2 formation using the $NaHCO_3$, implying the different mechanism compared to previous reports. The formation of H_2O_2 from H_2O causes the release of protons ($2H_2O \rightarrow H_2O_2 + 2H^+ + 2e^-$), which could significantly lower the local pH (ref. 13). The accumulated local protons would shift the H_2O-to-H_2O_2 equilibrium towards its reverse reaction. The 1.0 M Na_2CO_3 electrolyte (pH = 11.96) shows higher pH than 1.0 M $NaHCO_3$ electrolyte (pH = 8.2), which provides higher buffer capacity for the local environment. Thus, from a pH perspective, the Na_2CO_3 electrolyte might be more suitable for two-electron oxidation compared to $NaHCO_3$. However, we do not observe a direct connection between high pH and H_2O_2 selectivity. As a control experiment, we evaluated the performance in 1 M K_3PO_4 (pH = ~13.2) (Supplementary Fig. 7a) which has even higher pH than Na_2CO_3 but showed lower activity and selectivity towards H_2O_2.

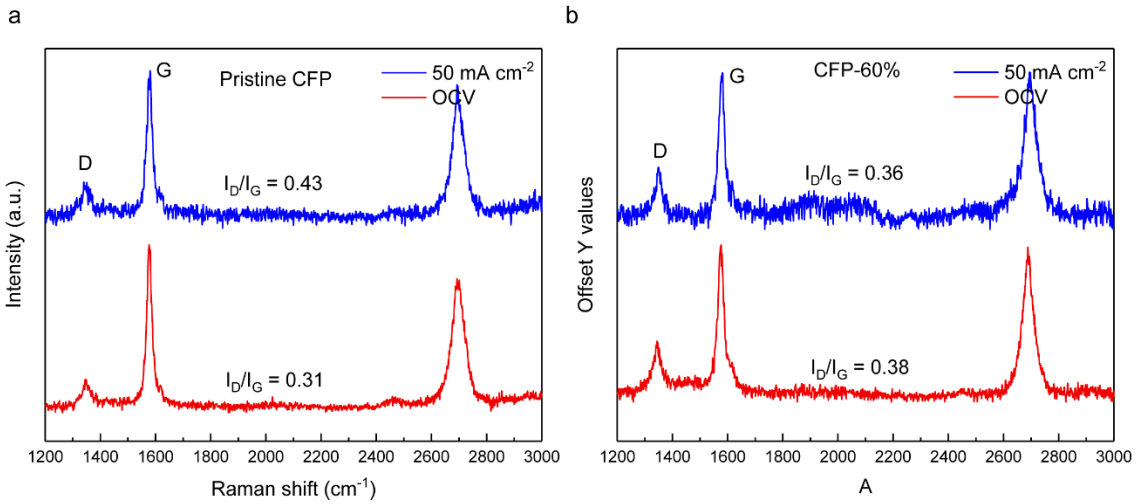

Supplementary Figure 10 | *Operando* Raman measurement of CFP based electrodes. **a**, Raman test of pristine CFP electrode under different condition in 1.0 M Na_2CO_3 electrolyte. **b**, Raman test of CFP-60% electrode under different condition in 1.0 M Na_2CO_3 electrolyte. OCV means open circuit voltage. The I_D/I_G ratio was calculated to illustrate the oxidation degree of carbon catalyst surface during electrolysis. Obviously, the reduced local H_2O concentration near the surface of CFP-60% catalyst, due to the trapped O_2 bubbles, can lead to a decrease of the oxidation of the graphene surfaces.

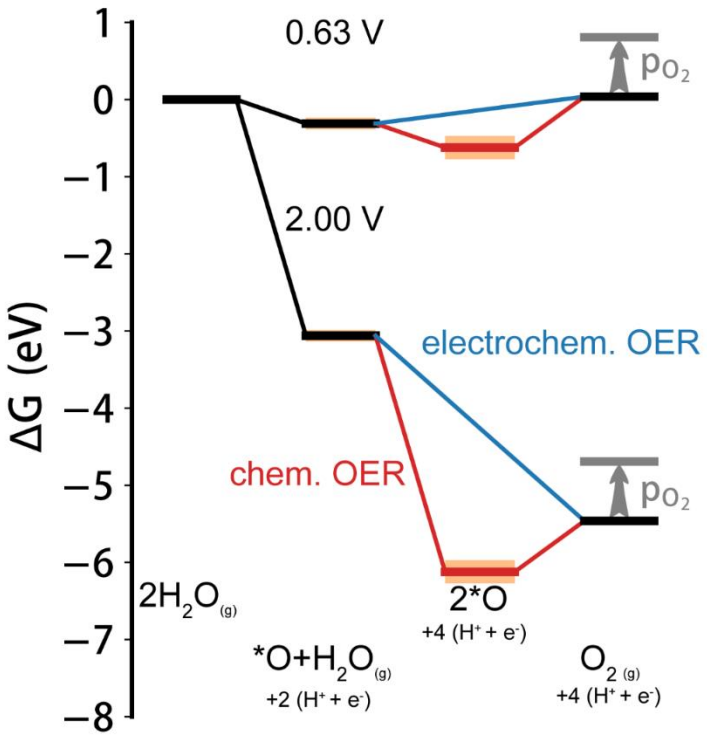

Supplementary Figure 11 | Free energy diagram of OER via surface bound *O intermediates. Shown are the average binding energies on the various graphene surfaces, the standard deviation is depicted with orange error regions. As seen from the diagram, the oxidation of water is strongly downhill at an applied potential of 2 V *vs.* RHE. This leads to the *O coverage being completely controlled by the water chemical potential. Consequently, even a large change of the O_2 pressure (indicated by the gray arrows) from 10^{-10} to 1000 bar has no direct influence on the *O coverage.

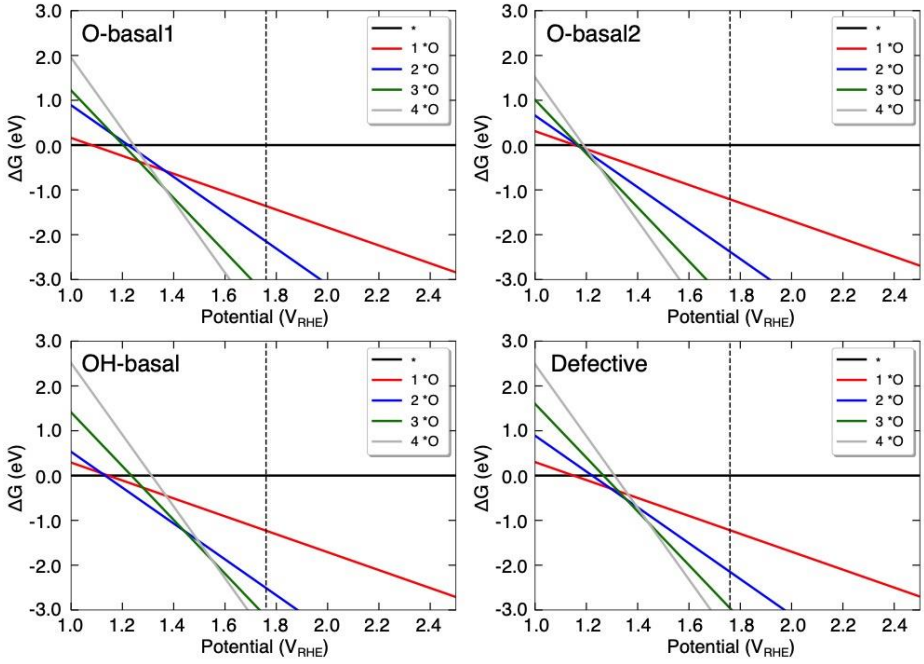

Supplementary Figure 12 | The surface Pourbaix diagrams of the defective graphenes.

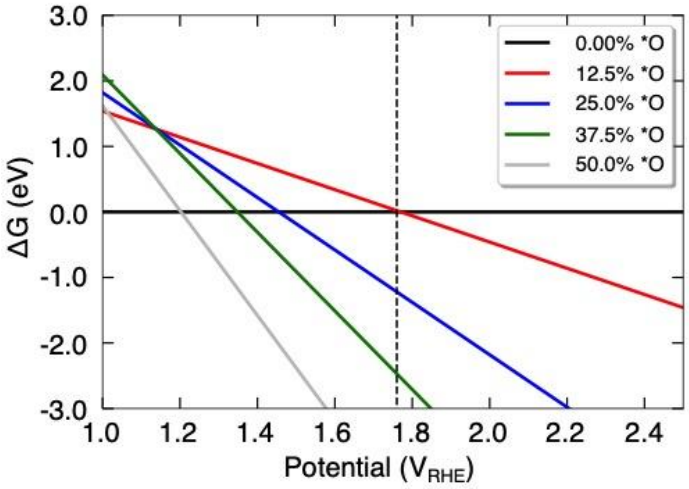

Supplementary Figure 13 | The surface Pourbaix diagrams of the graphene. 50 % *O corresponds to 4 adsorbed oxygen atoms in 8 carbon atom containing cell.

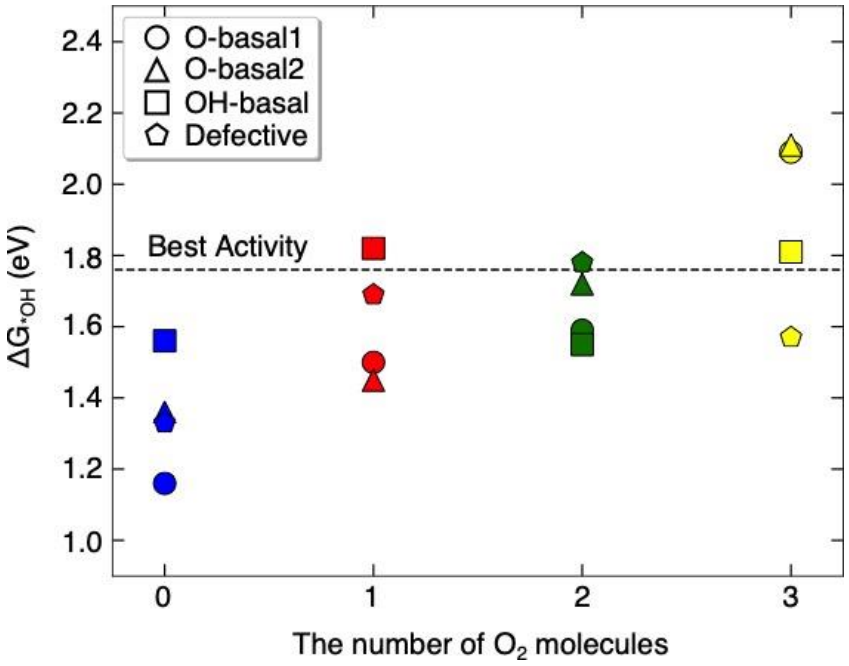

Supplementary Figure 14 | The calculated ΔG_{*OH} as a function of the number of oxygen atoms on the surface. We observed strengthening of ΔG_{*OH} as the number of oxygen atoms decreased. The dashed horizontal line is the ideal ΔG_{*OH} to achieve the highest activity and selectivity of H_2O oxidation to H_2O_2.

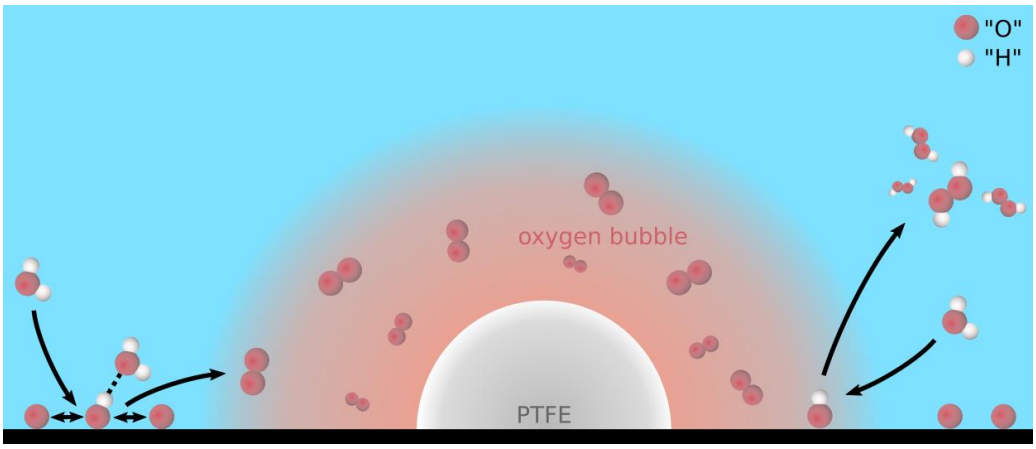

Supplementary Figure 15 | Schematic illustration of interfacial effects that explain the observed high hydrogen peroxide selectivity of our CFP-PTFE systems. The left side shows that the solvation stabilization may be decreased inside the oxygen bubble (right), since the presence of O_2 gas reduces the average number of possible hydrogen bonds. Further, we found experimental evidence for a more oxidized surface in the absence of the O_2 bubbles, which weakens *OH binding.

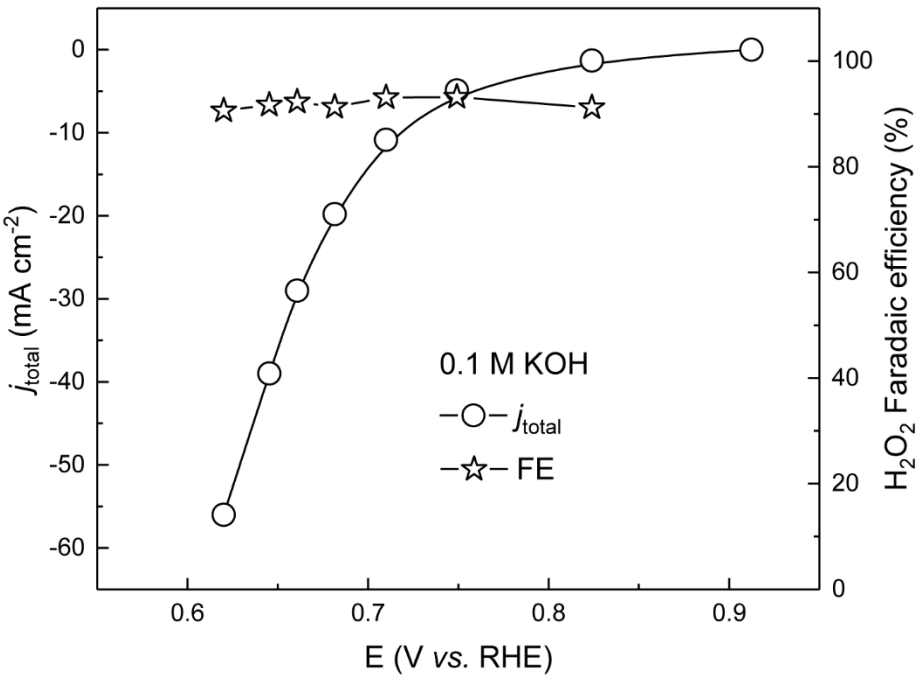

Supplementary Figure 16 | Two-electron oxygen reduction performance of oxidized carbon catalyst in 0.1 M KOH electrolyte.

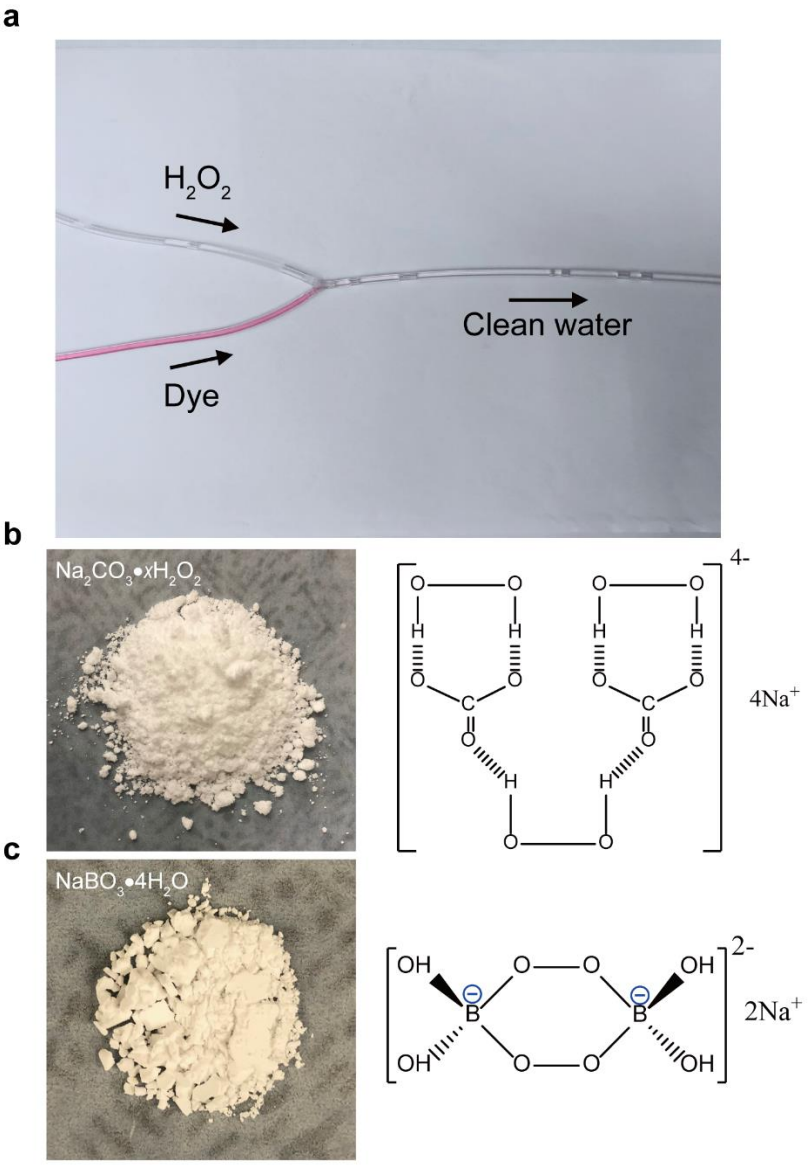

Supplementary Figure 17 | Application demos for our H_2O_2 electrosynthetic cell. a, digital photo of water treatment using *in-situ* produced H_2O_2 from our protype cell. The 50 ppm red Basic Fuchsin dye was immediately degraded when touches with the electrolyte from our $2e^-$-WOR//$2e^-$-ORR cell. **b**, digital photo of as-prepared solid H_2O_2 powder and the corresponding chemical structure. **c**, digital photo of as-prepared sodium perborate powder and the corresponding chemical structure.

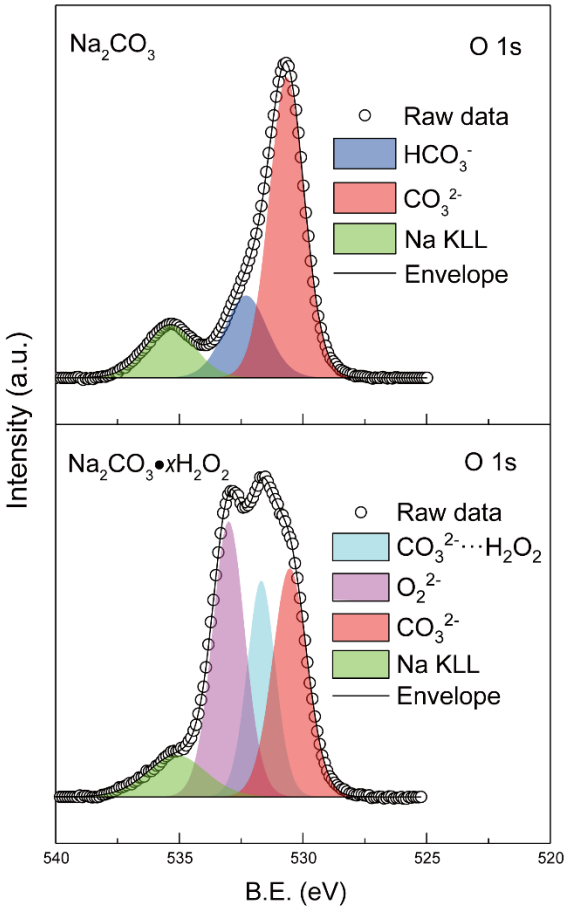

Supplementary Figure 18 | XPS analysis of commercial Na_2CO_3 (Sigma) and as-prepared solid H_2O_2 in our study, confirming the formation of $Na_2CO_3 \cdot 1.5H_2O_2$ adduct product. As shown in Fig. 3e, the O 1*s* peak of Na_2CO_3 can be deconvolved into three components at binding energies of 530.7, 532.3 and 535.4 eV. The strongest peak, which occurs at a binding energy of 530.7 eV, is due to the oxygen atoms in the CO_3^{2-} ions[5,6]. The peak centered at 532.3 eV reflects the structure of HCO_3^- ions[7]. The peak at 535.4 eV corresponds to Na KLL Auger emission[8]. For the extracted SPC ($Na_2CO_3 \cdot xH_2O_2$) compound, as illustrated in Fig. 3f, the O 1*s* region was deconvoluted into four contributions at 530.6, 531.7, 533 and 535.2 eV. Notably, the peaks locate at 530.6 and 535.2 eV are responsible for carbonate ions and Na Auger line, respectively. The new contribution at 533 eV originates from the peroxide ions in SPC[9,10], revealing the successful formation of solid H_2O_2. In addition, the peak at 531.7 eV is presumably due to the carbonate oxygen atoms hydrogen-bonded with hydrogen peroxide molecules[5,11].

Supplementary Note 1: Estimation of the cost for electrosynthesis of H_2O_2

Operation condition: 1.7 V (120 mA cm^{-2} for CFP-60%); 1.0 M Na_2CO_3 solution; Faradaic efficiency: 153%

$$n_{H2O2} = \frac{1\ kWh * 1.53}{1.7\ V * 2 * 96485\ C\ mol^{-1}} = \sim 16.8\ mol \qquad (1)$$

Thus, finally we can obtain ~16.8 mol (571.2 g) H_2O_2 using 1 kWh electricity. Assuming the price of renewable electricity is 3 cents/kWh[12], we can have a rough estimation of an operational cost *ca.* \$0.05/kg-H_2O_2. Please be noted that we only calculate the cost of energy input as a back-of-envelope estimation, no other cost associated with practical production was included. As a reference, the commercial H_2O_2 price is ~ \$1.5/kg-H_2O_2 plus transportation cost[13,14].

Supplementary Table 1. **Adsorption energy of *OH and *O reaction intermediates in vacuum and using various solvation approaches, explicit water molecules, implicit continuum water and a hybrid approach.** All energies are given in eV. The calculations were performed for 5555-6-7777 defective graphene. We tested various solvation approaches including explicit, implicit, and hybrid (explicit+implicit) solvation models. To investigate the impact of explicit solvation, we used a micro-solvation approach as demonstrated by Calle-Vallejo et al. (*J. Phys. Chem. C*, 2019, 123, 9, 5578-5582). This approach uses a limited number of water molecules around the active site to represent solvation effects from direct adsorbate-water interactions. The results are summarized in the table below. Implicit solvation can in principle predict solvation energies, but may under-predict hydrogen bond stabilization, because it is by construction a mean-field approach that does not describe dynamic, microscopic interactions. We see this in the case of *OH, where the additional stabilization due to hydrogen bonding is around 0.2 eV ("Explicit+Implicit") in comparison with the only 0.1 eV stabilization due to the dielectric background ("Implicit"). In the case of *O, only the dielectric background contributes to the solvation stabilization, giving a small total solvation energy of 0.1 eV ("Explicit+Implicit").

	Vacuum	Explicit	Implicit	**Explicit + Implicit**
G(*OH)	**1.39**	1.26	1.21	**1.05**
G(*O)	**2.28**	2.51	2.18	**2.20**

Supplementary References

1 Reshetenko, T. V. *et al.* Multi-Analytical Study of Gas Diffusion Layer PTFE Content Local Variation. *ECS Transactions* **50**, 591-599 (2013).

2 Ganguly, A., Sharma, S., Papakonstantinou, P. & Hamilton, J. Probing the thermal deoxygenation of graphene oxide using high-resolution in situ X-ray-based spectroscopies. *The Journal of Physical Chemistry C* **115**, 17009-17019 (2011).

3 Xu, L. *et al.* NOx sensitivity of conductometric In (OH) 3 sensors operated at room temperature and transition from p-to n-type conduction. *Sensors and Actuators B: Chemical* **245**, 533-540 (2017).

4 Figueiredo, J., Pereira, M., Freitas, M. & Orfao, J. Modification of the surface chemistry of activated carbons. *Carbon* **37**, 1379-1389 (1999).

5 Zhubrikov, A. *et al.* XPS characterization of sodium percarbonate granulated with sodium silicate. *Russian Journal of Inorganic Chemistry* **54**, 1455-1458 (2009).

6 Datsyuk, V. *et al.* Chemical oxidation of multiwalled carbon nanotubes. *Carbon* **46**, 833-840 (2008).

7 Shchukarev, A. & Korolkov, D. XPS study of group IA carbonates. *Open Chemistry* **2**, 347-362 (2004).

8 Tsai, F.-T., Wang, H.-C., Ke, C.-H. & Liaw, W.-F. FeCo/FeCoPxOy (OH) z as Bifunctional Electrodeposited-Film Electrodes for Overall Water Splitting. *ACS Applied Energy Materials* **1**, 5298-5307 (2018).

9 Ohno, T., Masaki, Y., Hirayama, S. & Matsumura, M. TiO2-photocatalyzed epoxidation of 1-decene by H2O2 under visible light. *J Catal* **204**, 163-168 (2001).

10 Ganguly, P. & Hegde, M. Evidence for double valence fluctuation in metallic oxides of lead. *Physical Review B* **37**, 5107 (1988).

11 Pritchard, R. G. & Islam, E. Sodium percarbonate between 293 and 100 K. *Acta Crystallographica Section B: Structural Science* **59**, 596-605 (2003).

12 Chu, S., Cui, Y. & Liu, N. The path towards sustainable energy. *Nature materials* **16**, 16 (2017).

13 How much does H_2O_2 cost? *http://www.h2o2.com/faqs/FaqDetail.aspx?fId=25*.

14 Fuku, K., Miyase, Y., Miseki, Y., Gunji, T. & Sayama, K. Enhanced oxidative hydrogen peroxide production on conducting glass anodes modified with metal oxides. *Chemistryselect* **1**, 5721-5726 (2016).